Journal of The
Electrochemical Society

New Insights to Electrolyte Design for Aqueous Zinc-Manganese Dioxide Batteries: The Role of Anion Complexes and pH Dynamics

To cite this article: J. Pross-Brakhage *et al* 2025 *J. Electrochem. Soc.* **172** 050513

Journal of The Electrochemical Society, 2025 **172** 050513

New Insights to Electrolyte Design for Aqueous Zinc-Manganese Dioxide Batteries: The Role of Anion Complexes and pH Dynamics

J. Pross-Brakhage,[1,z] J. Meyer,[1] C. Mehlich,[1] O. Fitz,[2] and P. Birke[1]

[1]*University of Stuttgart, Institute for Photovoltaics, Chair for Electrical Energy Storage Systems, Stuttgart 70569, Germany*
[2]*Department of Electrical Energy Storage, Fraunhofer Institute for Solar Energy Systems ISE, Freiburg 79110, Germany*

Electrolytic zinc manganese dioxide batteries (ZMB) are promising alternatives to lithium-ion systems due to their cost-effectiveness, material abundance, and safety, but their adoption is hindered by challenges in energy density and stability. To overcome these hurdles, a deeper understanding of the underlying electrochemical processes is required. This study investigates the role of acetate and sulfate anions in electrolyte performance, focusing on pH buffering capacity and complexation effects at the electrode interface. A thermodynamic model was developed to simulate speciation and reaction equilibria, highlighting that proton transport is the rate-limiting step in sulfate-based electrolytes. Acetate-containing electrolytes exhibited superior buffering capacity and facilitated proton-coupled electron transfer, leading to enhanced manganese dioxide deposition at moderate pH levels. For the first time, a systematic study was conducted in which sulfate was progressively substituted by acetate while maintaining consistent pH conditions. Although acetate ions enable cyclability under mild pH conditions, their strong complexation with Mn^{3+} promotes manganese diffusion into the electrolyte, ultimately reducing reversibility as acetate content increases. Moreover, contrary to common assumptions, acetate anions do not inherently enhance anode stability under identical pH conditions. These insights provide a foundation for optimizing electrolyte design to overcome the limitations of zinc-manganese dioxide batteries.
 [DOI: 10.1149/1945-7111/add387]

Manuscript submitted February 25, 2025; revised manuscript received April 29, 2025. Published May 13, 2025.

Supplementary material for this article is available online

Batteries based on zinc and manganese dioxide have come to the fore especially because of cost, availability of active materials and safety.[1] Nevertheless, the underlying energy storage mechanisms of manganese dioxide (MnO_2) in zinc manganese dioxide batteries (ZMB) with mildly acidic aqueous electrolytes remain poorly understood and there is still a great debate within the research field regarding the exact mechanisms involved. An improved understanding will be the key to success tackling existing challenges related to long-term stability and energy density. At the positive electrode, the intercalation of zinc ions (Zn^{2+}) or protons (H^+) and the deposition of manganese dioxide are primarily discussed.[2,3] One reason for the ongoing uncertainty could be the difficulty that classic material characterization methods like X-ray diffraction (XRD) reach their limits. Various publications show that the same characterization methods lead to different interpretation due to similar layered structures and overlapping material-characteristic peaks which can be assigned to either different zinc-containing manganese oxide species resulting from the intercalation of Zn^{2+}, or the formation of zinc hydroxide sulfate (ZHS) species which are seen in connection with proton-coupled mechanisms like manganese dioxide deposition.[4–6]

Nevertheless, discussions so far have already received a general consensus that the MnO_2/Mn^{2+} redox reaction serves as a contributor to the battery's capacity at the positive electrode, although its precise contribution remains unclear.[7–9] The Mn^{2+}/Mn^{4+} deposition mechanism electrode offers significant potential for enhancing energy density, owing to its two-electron transfer process and higher voltage compared to the Zn^{2+} insertion mechanism.[10] Consequently, it is essential to explore the factors that can increase the contribution of this mechanism to overall battery performance.

The choice of electrolyte composition plays a crucial role in ZMBs because it not only serves to ionic charge transport between the electrodes but also actively participates in the chemical reaction. During charging, the dissolved ions are deposited, while during discharging, they dissolve back into the electrolyte, ensuring the continuous operation of the battery. Therefore, the active salt concentration in the electrolyte also determines the achievable energy density. Furthermore, the properties of the anions play a crucial role, and their influence on cell performance has been extensively studied.[11–13] The addition of chloride-containing salts has raised concerns about the formation of toxic chlorine gas, and studies have shown that the Cl^- anion accelerates anode corrosion.[14,15] While some researchers have demonstrated performance advantages of electrolytes such as $Zn(OTF)_2$ and $Zn(TFSI)_2$, their high cost may limit commercial applicability.[16–18] Instead, the use of sulfate and acetate salts to introduce the relevant cations, Zn^{2+} and Mn^{2+}, has proven to be the most suitable approach, making them the most frequently used electrolyte basis in the literature.

Regarding the role of anions, it is often stated that they profoundly change the storage mechanism, turning the intercalation/de-intercalation behavior in sulfate-based electrolytes into the deposition mechanism in acetate-based electrolytes.[2,13,19–23] This change of reaction pathway is assigned to the coordination of CH_3COO^- (hereinafter abbreviated as Ac^- ions) with Mn^{2+} ions which enables the direct deposition on the electrode. Thus, a higher reduction potential is observed in acetate-based electrolytes for MnO_2 deposition/dissolution, while the lower reduction peak in sulfate-based electrolytes is attributed to insertion mechanism of Zn^{2+} and H^+ into the MnO_2 cathode.[20–22] These effects and their implications on battery performance will be explored and discussed in more detail in the following sections.

Since the deposition of MnO_2 is a proton-coupled electron transfer (PCET) reaction, the pH of the electrolyte solution has also a decisive influence, and it was demonstrated that the reaction mechanism is strongly dependent on the present pH value of the electrolyte and the local pH conditions at the electrodes.[24] Some publications have shown that the proportion of manganese dioxide deposition in sulfate electrolyte increases with increasing proton concentration.[25–27] Operation in the acidic pH range, however, leads to severe stability problems of the zinc anode, which results in corrosion and hydrogen evolution.[10] Kim et al. show that the Brønsted acidity of metal aqua complexes itself can serve as a proton source to a certain extent and, moreover, the precipitation of ZHS can assist the dissolution-deposition mechanism but has a low pH-buffering capacity in the pH range considered, resulting in high overpotentials and sluggish reaction kinetics.[10,28,29] It is shown that, in contrast, the acetate ion is able to create a stable proton

[z]E-mail: julia.pross-brakhage@ipv.uni-stuttgart.de

environment in mild pH through its acid-base characteristic and therefore facilitates the electrolytic mechanism at the positive electrode.[30–32] This ability is also cited as the reason the acetate ion is said to improve the stability of the negative electrode, which leads to reduced corrosion and dendrite formation.[13,20,25,33–35]

It can be summarized that the processes at the positive electrode are governed by thermodynamic processes, highlighting the need to develop a fundamental understanding of the coupled effects between the electrolyte's pH and the formation of complexes. Although it is known that these homogeneous complexation reactions play a crucial role, their influence on electrolytes of ZMB has not yet been investigated in detail on a theoretical basis. This study aims to systematically examine the impact of acetate and sulfate anions on the reaction mechanism, with a particular focus on their interplay with the pH and the complexation behavior. To address this, controlled experimental conditions are employed, minimizing the influence of mass transport limitations. A thermodynamic model is developed and validated through titration experiments to map complexation behavior, providing a theoretical foundation. In previous studies, acetate and sulfate electrolytes have often been compared by different pH values, making it difficult to isolate the independent effects of the pH. Unlike previous research, this study explores the full salt concentration range and considers the effects of the complexation and the pH on the reversibility of the processes. Furthermore, to the best of our knowledge, it is the first study to systematically investigate both the anion-specific and the pH-dependent effects on the anode.

Methods

Materials and solutions.—All the chemicals were analytical grade and used without further purification. Zinc sulfate heptahydrate ($ZnSO_4{\cdot}7H_2O$ >99.5% purity), manganese(II)-sulfate monohydrate ($MnSO_4{\cdot}H_2O$ >99% purity), manganese(II)-acetate tetrahydrate ($MnAc_2{\cdot}4H_2O$ >99% purity) and zinc acetate dihydrate ($ZnAc_2{\cdot}2H_2O$ >99% purity) were purchased from Carl Roth (Germany). Sodium hydroxide (NaOH, 98% purity) was purchased from ITW Reagents (Germany). Sulfuric acid (H_2SO_4, 96% purity) was obtained from Alfa Aesar (UK). All solutions were prepared immediately before the experiments using ultra-pure water. To systematically examine the impact of anions, six electrolytes with varying ratios of $MnSO_4$, $ZnSO_4$, $MnAc_2$, and $ZnAc_2$ were prepared and illustrated in Fig. 1. During the preparation of electrolytes for electrochemical measurements, particular attention was paid to avoiding the contamination of foreign ions, such as Na^+, as previous studies have demonstrated that these can significantly affect electrochemical properties.[36] The concentration of active materials (Mn and Zn) was maintained at a constant value of 1 M, while the ratio of acetate to sulfate ions varied across the full range, from purely sulfate-based to purely acetate-based salts. This type of preparation also ensures that the ionic strength remains relatively constant. For the characterization of the physicochemical properties, the electrolytes are used without pH adjustment, whereas for electrochemical measurements, a concentrated solution of 2 M H_2SO_4 is used to reach the exact targeted pH of 4, 4.5 and 5.

Potentiometric titration.—To investigate the buffer capacity of the various electrolytes, potentiometric titrations were carried out. A highly concentrated solution of 10 M NaOH is used to minimize the effect of dilution by the addition of titrant. To approximate perfect mixing, the solution was stirred with a magnetic stirring bar of 3 cm on a magnetic stirrer at approximately 400–500 rpm. A Mettler Toledo InLab Micro Pro-ISM probe was used for pH measurements and calibrated before use with 2.00, 4.00, 7.00, and 10.00 pH buffers from Carl Roth (Germany). The pH was recorded with Mettler Toledo Seven Compact Duo S312. This is also used to determine the ionic conductivity of the different electrolytes.

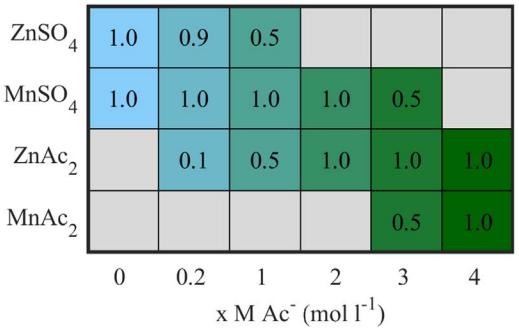

Figure 1. Composition of electrolyte variants with varying ratios of components ($MnSO_4$, $ZnSO_4$, $MnAc_2$, $ZnAc_2$).

Electrochemical methods.—Electrochemical measurements was carried out in a cuvette cell with 4 ml electrolyte volume. For all experiments, the BasyTec (Germany) battery test system was used. A carbon paper (280 μm, Sigracet 39AA, SGL Carbon, Germany) served as the current collector for the positive electrode and a zinc foil (250 μm, 99.95%, Thermo Fisher Scientific, Germany) as the negative electrode. The wetted, active area of the electrodes is 3.5 cm^2. The MnO_2 is in situ deposited on carbon paper during the first charging process. A silver/silver chloride (Ag/AgCl) reference electrode (RE-1BP, ALS, Japan) was used as the reference electrode for open circuit potential measurements. For measuring the open circuit voltage while GITT, a relaxation period of one hour was implemented to ensure that the pH gradients within the cell have equalized. A magnetic stirring bar with a diameter of 2 mm from ROTILABO was used for the in situ measurements. All experiments were carried out at room temperature (22 °C ± 2 °C).

Model theory and governing equations.—To represent the complex properties of the electrolyte, a thermodynamic model was created based on the law of mass action. The law of mass action is a widely accepted formulation for chemical equilibrium, assuming infinitely fast reactions, which implies that the participating ions are locally in chemical equilibrium with one another. The reaction for the hydrolysis of Zn^{2+}, for example, can be formulated as follows:

$$Zn^{2+} + H_2O \rightarrow Zn(OH)^+ + H^+ \quad [1]$$

The law states that if the system is in equilibrium, then the ratio K_{eq}^0 is constant:

$$\frac{[Zn(OH)^+]\ \ [H^+]}{[Zn^{2+}]} = K_{eq}^0 = 10^{-8.99} \quad [2]$$

Here, square brackets denote molar concentration in $mol.l^{-1}$ (M). Since the concentration of water is very high compared to the reactants it is assumed to remain virtually unchanged and therefore is omitted from the mass action expression as is common practice.[37] In systems that deviate from ideal dilution, as is the case here, equilibrium expressions should formally be written in terms of activities, where $a_S = \gamma_S[S]$, with γ_S representing the activity coefficient. However, in concentrated multicomponent systems, the reliable determination of ion-specific activity coefficients is highly challenging and remains an active area of research. Moreover, it is necessary to rely on semi-empirical models, whose parameterization involves substantial experimental effort.[38]

As an alternative, we adopt the widely used approach of employing concentration-based equilibrium constants $K_{eq}(I)$ which are defined at the ionic strength relevant to the system.[38] This allows equilibrium expressions to be written in terms of concentrations (see Eq. 2), with non-ideal behavior implicitly incorporated through the experimental determination of the constants. In this study,

equilibrium constants were obtained via potentiometric titrations of the relevant electrolytes and their mixtures. The resulting titration curves were compared with model predictions to validate the selected constants, following procedures well established in the literature.[39,40] Although a detailed activity-based model could provide further insight, its development lies beyond the scope of the present study.

A total of 29 species are involved in 24 chemical reactions, with their equilibrium constants summarized in Table S1. These species are all derived from five key components: Zn^{2+}, H^+, Mn^{2+}, SO_4^{2-}, and Ac^-. In acid-base reactions, the reacting species are conserved, allowing for the definition of a mass balance for each of the five components. For the total concentration of zinc $c_{T,Zn}$, for example, this results in:

$$c_{T,Zn} = [Zn^{2+}] + \sum_{l=1}^{2} [Zn\ (SO_4)_l^{2(1-l)}] + \sum_{k=1}^{2}\sum_{l=1}^{4} k\ [Zn_k(OH)_l^{(2k-l)}] + \sum_{l=1}^{3} [Zn\ (Ac)_l^{(2-l)}] \quad [3]$$

Where l denotes the number of anions bound to the Zn^{2+} and k corresponds to den number of Zn^{2+} in each species. The law of mass action can also be applied to the precipitation of solid species. The precipitation and dissolution of each solid species can be calculated using the saturation index (SI), which relates the actual ion activity product to the solubility constant. To solve the equilibrium model, an additional conditional equation must be set up, for which three main approaches exist: charge balance, proton mass balance and alkalinity. Each of these approaches is theoretically justified and has been successfully implemented in numerical calculations of chemical equilibria.[41] In this case, the proton mass balance is chosen, as it explicitly accounts for the formation and consumption of H^+ and enables efficient integration of the model. This results in a non-linear system of equations that is solved in MATLAB using Newton-Raphson method with the constraint suggested by Carrayrou and coworkers.[42,43]

Results

The influence of the anion and the pH value on the performance of the ZMBs is investigated through both experimental measurements and modeling. Firstly, the influence of metal complex formation on key physicochemical properties is investigated. Following this, its impact on the equilibrium potential is analyzed and the distinct role of anions on mass transport in operation is explored. Subsequently, these findings are extended to investigate how varying anion compositions and pH levels shape the system performance. Finally, the influence of these factors on the zinc anode stability is assessed.

Influence of the metal complexes on the acid-base behavior.— To understand the influence of complex formation on electrochemical behavior, it is essential to analyze the complexes present in the electrolyte (Fig. 2). At the given salt concentrations, metal ions predominantly exist as complexes, where they are bound to ligands through short-range, non-directional electrostatic interactions.[44] For example, in 1 M zinc sulfate electrolyte (Fig. 2a), Zn^{2+} can be found as a free ion, as a neutral species ($ZnSO_4^0$), or as a complex anion ($Zn(SO_4)_2^{2-}$). Although hydroxo complexes also form, their concentrations are very low and are therefore omitted from the illustration but still included in the calculations.

The strong polarization of coordinated water molecules by Zn^{2+} leads to proton dissociation, contributing to the acidic behavior of sulfate-based electrolytes. As a result, salts derived from strong acids, such as $ZnSO_4$ and $MnSO_4$, exhibit weak acidity (Fig. S1), with pKa values of 8.96 and 10.59, respectively. However, reported pH values vary in the literature, likely due to residual free acid or differences in the commercial sources of the salts.[45,46] In contrast, acetate-based electrolytes tend to have higher pH values due to the basic character of the acetate anion (pKb = 9), which counteracts hydrolysis effects.[46] Consequently, even a partial substitution of sulfate with acetate shifts the pH toward a nearly neutral range (Fig. S1). For clarity, Fig. 2 illustrates the zinc speciation in a 1 M $ZnSO_4$ + 1 M $MnSO_4$ solution, while the manganese speciation under the same conditions is provided in Fig. S2. Additionally, salt precipitation occurs above certain pH thresholds: ZHS precipitates at pH just above 5, while the analogous salt of acetate zinc hydroxy acetate (ZHA) forms only at pH values exceeding 6.[47]

To characterize the acid-base behavior, potentiometric titrations are a widely used method, which are also employed here to validate the model. The acetate salts are also often ascribed to the buffer property of the associated acetic acid (HAc). As shown in Fig. 3a for $ZnAc_2$ and HAc, the model is capable of replicating the acid-base behavior within the range of the measurement accuracy (± 0.09 pH), confirming that it captures the key thermodynamic behavior of the system and is therefore suitable as a basis for interpretation. A similar behavior can be observed for manganese acetate (Fig. S3). According to the titration curves, a shift in pH for zinc acetate curves to lower pH is visible, compared to the titration curve with acetic acid. The shift in buffering behavior occurs due to the formation of complexes between Zn^{2+} and Ac^-.[39] This shift becomes more apparent when we examine the speciation for HAc (top) and $ZnAc_2$ (bottom) in Fig. 3c. The buffering action of HAc relies on the formation of complexes between Ac^- and H^+, which is in direct competition with the complexation of Ac^- with Zn^{2+}. [46] As a result, the equivalence point of HAc, where half of the acid is deprotonated, shifts to a lower pH when Zn^{2+} is present (indicated by the arrow and hatched area).

To further analyze the effects, the buffer capacity β is an interesting parameter, which defines the ability of a buffer to stabilize the pH value despite the addition of acid or base and is determined as follows:

$$\beta = \frac{d[OH^-]}{d\mathrm{pH}} \quad [4]$$

The shift in the effective range of HAc and $ZnAc_2$ can be seen even more clearly from Fig. 3b. Additionally, significant differences for sulfate-based electrolytes is visible, which clearly shows that the pH stabilization capacity of zinc sulfate is several orders of magnitude lower, until the point where the precipitation of ZHS causes an additional buffering effect. Only in the acidic pH range (pH <2) buffering capacities become comparable. This is also the pH range in which publications have shown that the contribution of MnO_2 deposition to the overall reaction increases in sulfate-containing electrolytes. However, it has been shown that anode stability decreases dramatically at a value below pH 4.[48] At the same time, the probability of the formation of further manganese and zinc-containing solid species such as $ZnMn_2O_4$ and MnOOH increases from a pH > 4.7, which can lead to capacity fade.[49] This suggests that operating within the pH range of 4 to 5 is optimal. However, due to the shift in buffering behavior between pH 4 and 5, $ZnAc_2$ exhibits a 40% lower buffering capacity compared to HAc (Fig. 3b). This significant effect, which arises from the complexation of Zn^{2+} with acetate ions, has not yet been discussed in the literature regarding the selection of pH buffers for ZMBs. The complexation reduces the effectiveness of the acetate buffer in stabilizing the pH within the target range, making it less effective at maintaining pH stability. This highlights that not only acid dissociation constant, but also the stability constants of the complexes formed must be considered when selecting suitable buffering agents. Thermodynamic considerations, as presented in this work, could therefore provide valuable insights for choosing appropriate anions for ZMB electrolyte systems.

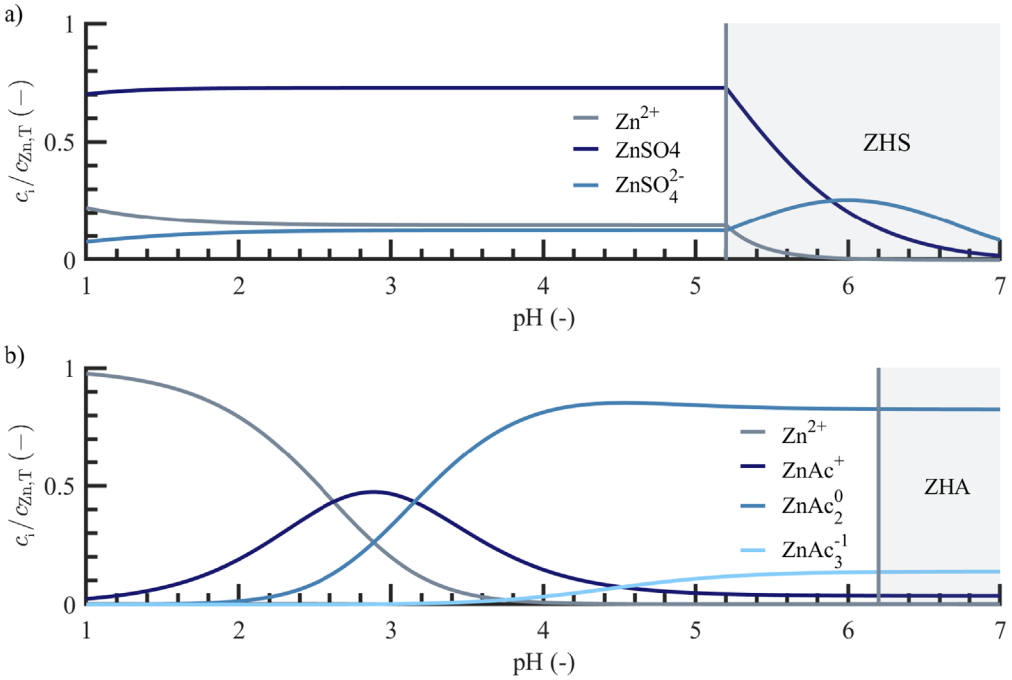

Figure 2. Speciation diagrams of zinc complexes in (a) sulfate-based and (b) acetate-based electrolytes as a function of pH. The shaded areas indicate the precipitation of ZHS and ZHA.

Influence of anion type and pH on equilibrium potential.—In the literature so far, it is often suggested that different anions (such as sulfate and acetate) lead to distinct reaction mechanisms, as the reaction can be observed at different potentials.[2,13,19,20,22] This phenomenon is attributed to the altered complexation behavior of Ac^- with Mn^{2+}, which is believed to facilitate the direct deposition of manganese dioxide at a lower potential. In the following section, this hypothesis will be examined by incorporating the knowledge of the speciation from model as a function of pH into the Nernst equation to determine the equilibrium potential and comparing the results with experimental measurements. Although this approach has been applied to other battery types, it has not yet been investigated for the present cell chemistry to the best of our knowledge,[50,51] For the ZMB system, the positive electrode potential can be calculated as follows:

$$E_p = E_p^0 + \frac{RT}{zF} \ln\left(\frac{c_{H^+}{}^4}{c_{Mn^{2+}}}\right) \quad [5]$$

Here, E_p^0 is the standard potential for the MnO_2/Mn^{2+} redox couple (+1.23 V vs SHE), R is the gas constant, T is the temperature, z is the number of electrons transferred during redox reaction, F is Faraday's constant, and c is the concentration of the respective ions. For the negative electrode, the equation results accordingly:

$$E_n = E_n^0 + \frac{RT}{zF} \ln\left(c_{Zn^{2+}}\right) \quad [6]$$

Where, E_n^0 is the standard potential for the Zn^{2+}/Zn redox couple (−0.76 V vs SHE). The total open circuit voltage (OCV) results from the difference between the individual electrode potential to:

$$OCV = \quad E_p - E_n \quad [7]$$

For a meaningful comparison of the influence of anions and pH, it is essential to maintain consistent conditions and evaluate the system under equilibrium, excluding kinetic influences. For this, five cycles with an areal current of 0.06 mA.cm^{-2} and an areal capacity 0.06 mAh.cm^{-2} are performed at pH 4.5. Afterwards, the pH is adjusted using H_2SO_4 and NaOH, and the voltage is measured after a relaxation time of 15 min. Figure 4a shows the measured variation of the open-circuit voltage (OCV) as a function of pH for the acetate-based electrolyte. For comparison, the predicted potential based on Eqs. 5–7 is depicted as a gray line, which does not account for complexation effects. It is evident that including complexation reactions significantly improves the alignment with the experimental data. This is reflected in the root mean squared error of 18 mV for the full-cell potential over the pH range of 2 to 6, indicating that the inclusion of complexation reactions provides a much more accurate representation of the observed behavior. It should be noted that the speciation model used here relies on concentration-based equilibrium constants and further refinement could be achieved using an activity-based electrolyte model, especially under high ionic strength conditions.

Figure 4b displays the measured potential of the negative zinc electrode against Ag/AgCl reference electrode at different pH values, where the influence of complex formation is clearly observable. The previous section demonstrated that in the pH range of 2 to 4, the concentration of free Zn^{2+} continues to decrease due to complexation with acetate ions (Fig. 2a), leading to a corresponding decrease in the potential of the negative electrode. For the sulfate-based electrolyte, the model consistently overestimates the voltage slightly (Fig. 4c). This suggests that a larger fraction of Zn^{2+} remains uncomplexed than the model assumes. Figure 4d compares the two voltage curves along with their respective accuracy. Although the potential for pH $<$ 3.5 is slightly lower for the acetate-based electrolyte, the accuracy of both curves overlaps for pH $>$ 3.5, indicating that they can no longer be distinguished based on complexation effects.

In the next step, semi-equilibrium conditions are examined using the galvanostatic intermittent titration technique (GITT) in ZMB full cells. This method consists of a sequence of ten current pulses for charge and discharge with 6 min with 0.06 mA cm^{-2}, each followed by a one-hour relaxation period during which no current flows through the cell, allowing the voltage to stabilize at equilibrium. To minimize the influence of mass transport during the short current pulses and ensure a uniform ion concentration within the electrolyte, stirring is employed using a magnetic stirring bar for forced

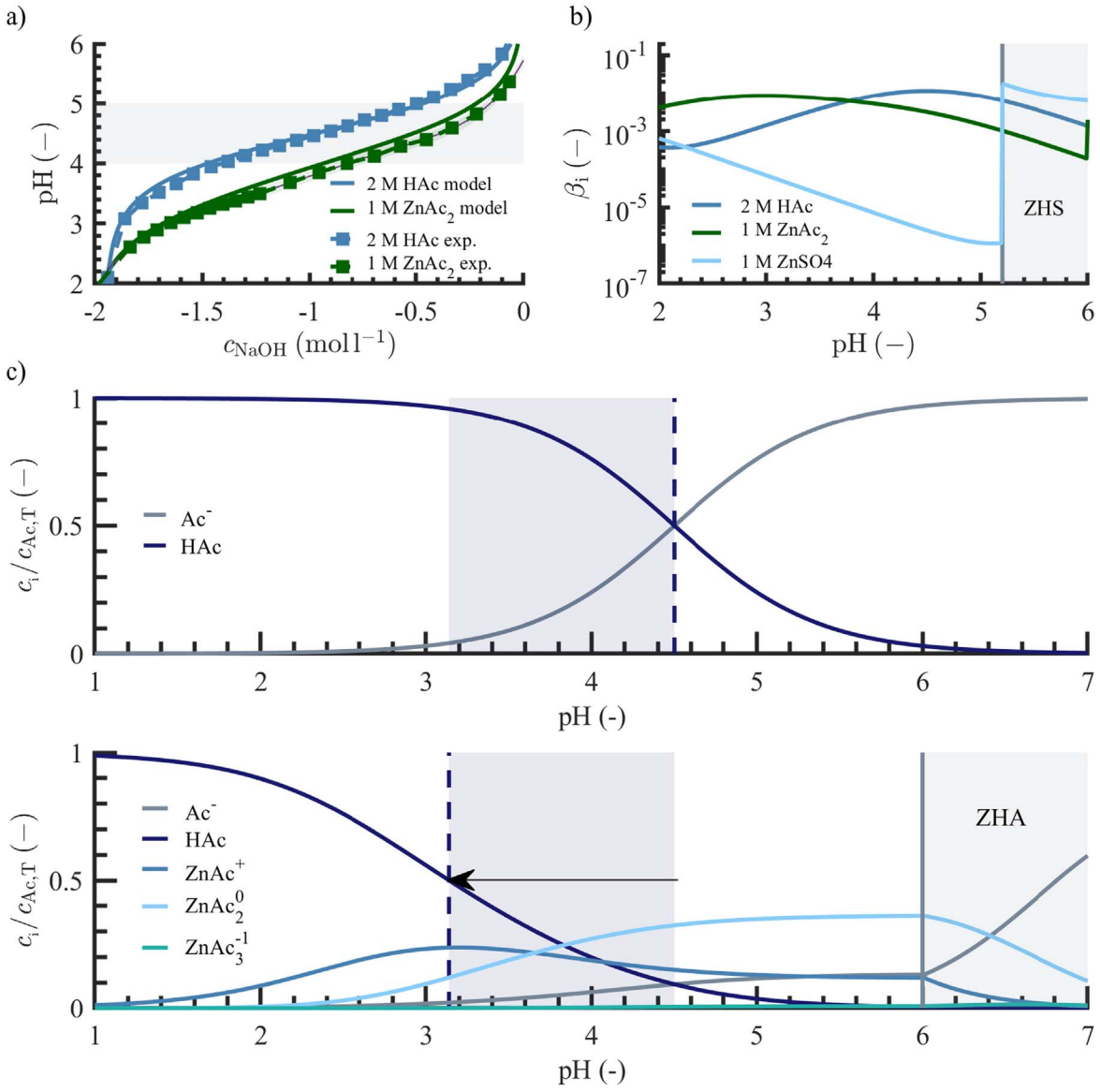

Figure 3. Model validation and shift of buffer capacity for 1 M ZnAc2 against 2 M HAc (a) Validation of Titration experiments with model for 2 M HAc and 1 M $ZnAc_2$ (b) Modeled buffer capacity for 2 M Hac, 1 M ZnAc2 and 1 M ZnSO4 (c) Speciation analysis showing a shift in the buffer behavior due to the presence of zinc-acetate complexes.

convection. Additionally, a pH electrode is placed between the electrodes to monitor the proton concentration.

Figure 5a shows the GITT measurements for sulfate- and acetate-based electrolytes at an initial pH of 4.5. In the acetate electrolyte, the voltage stabilizes after the relaxation period during charging and discharging. In contrast, for the sulfate electrolyte, a change in potential is observed during charging and discharging. In the next step, the pH change is investigated as a possible cause for this behavior. Figure 5b presents the pH values after relaxation. The pH changes in the opposite direction to the potential: a decrease in pH is observed during charging, followed by an increase during discharging. This suggests that the pH fluctuation is linked to the charge/discharge process. To eliminate the pH influence, the Nernst equation for MnO_2 deposition reaction is applied (Fig. 5b). This analysis shows that, after accounting for pH, the potential for both electrolytes remain nearly constant. The measured potential agrees within an average deviation of 10 mV, which is within accuracy range of the model for the open-circuit potential. Although we have not yet found a conclusive explanation for the voltage dip observed during discharge in the sulfate-containing electrolyte between 30% and 10% SoC, it appears that the voltage behavior for both electrolytes can be explained by the deposition reaction mechanism. Overall, these results suggest that, in the present experiments, the equilibrium voltage is more sensitive to pH than to the anion type, emphasizing the dominant role of pH in influencing electrochemical behavior.

Since the deposition of MnO_2 is a proton-coupled reaction, protons are added to the electrolyte during charging and are re-stored during discharging. Therefore, a parallel can be drawn to the titration experiments from the previous section, where the converted protons can be assigned to an equivalent amount of added sulfuric acid. This conclusion is further supported by the fact that the measured coulombic efficiency is almost 100% under the given conditions. Therefore, the addition or removal of protons through MnO_2 deposition will be simulated by the titration of a 2 M H_2SO_4 solution in the following experiments:

Figure 6a presents the results of titrations for an electrolyte with 1 M $ZnSO_4$ and 1 M $MnSO_4$, compared with the model. Although the qualitative trend is well represented, the pH decreases slightly more slowly in the titration experiment than predicted by the model.

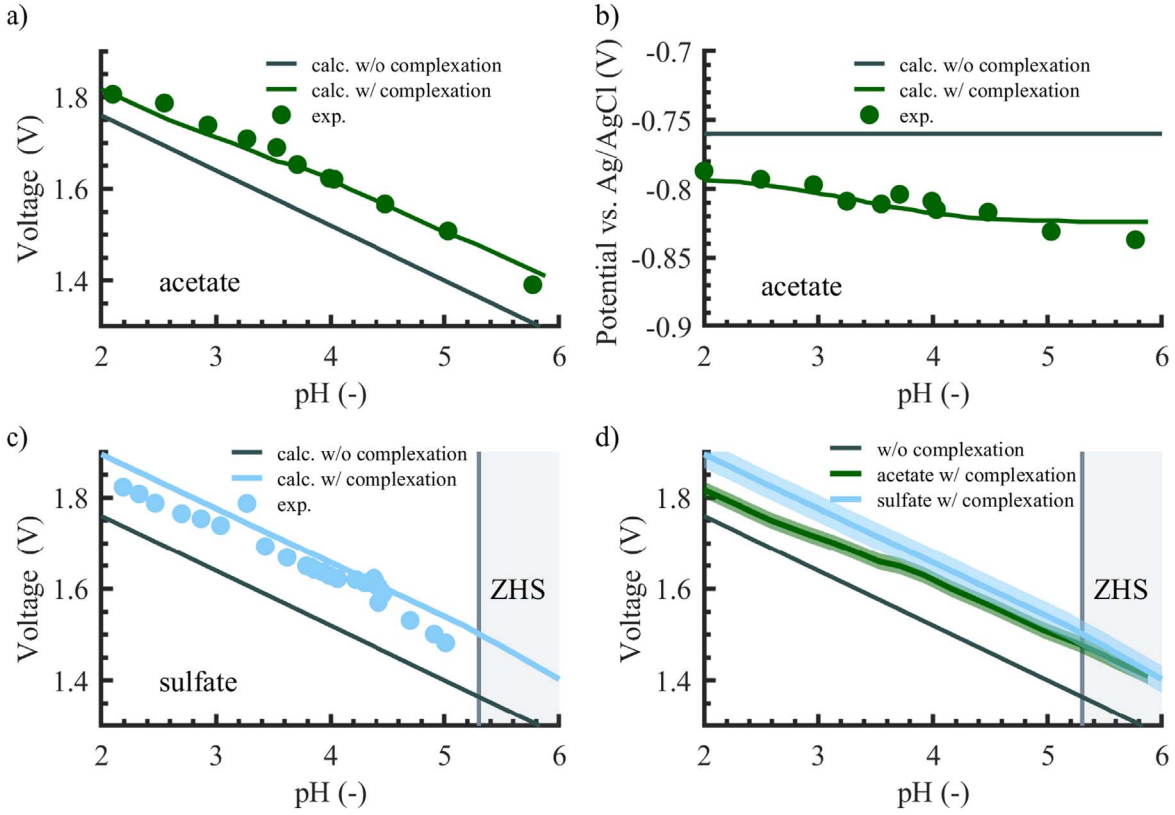

Figure 4. Validation of model calculations with experimental data for open-circuit voltage measurements. (a) Full-cell voltage as a function of pH for an acetate-based electrolyte (4 M Ac^-), comparing experimental data with model calculations, both with and without complexation. (b) Zinc electrode potential vs Ag/AgCl reference electrode in the acetate-based electrolyte (4 M Ac^-), highlighting the effect of complexation. (c) Full-cell voltage for a sulfate-based electrolyte (0 M Ac^-), comparing experimental results with model predictions. (d) Comparison of acetate (4 M Ac^-) and sulfate (0 M Ac^-) electrolytes, illustrating the impact of complexation on voltage. The shaded regions represent the mean error deviation between experimental data and model calculations.

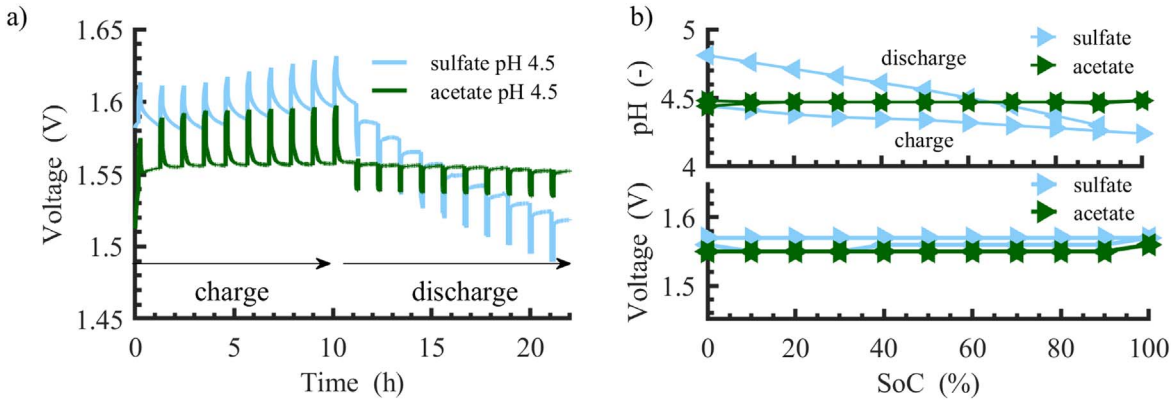

Figure 5. Open circuit voltage analysis for semi-equilibrium conditions. (a) GITT measurement for sulfate (blue) and acetate (green) at pH 4.5, showing voltage evolution during charge and discharge. (b) Top: pH after relaxation during charge and discharge. Bottom: Voltage corrected for pH effects, showing similar open-circuit voltages for both anions.

Since the electrolyte has very little buffering capacity in this pH range of ~3–5, even small differences lead to noticeable pH changes. When compared to the GITT measurements, a significantly lower pH is observed. This could indicate the occurrence of additional reactions that release fewer protons. Alternatively, it may suggest that protons are being bound either by surface hydroxyl complexation on the manganese dioxide[52] or through hydrogen evolution at the zinc electrode.

To investigate these hypotheses, the titration is repeated with the same electrolyte, where the respective electrodes are placed in the electrolyte during the titration process. The pH behavior during titration with the zinc negative electrode aligns well with the observations from the GITT measurements. The hydrogen evolution during the titration, which leads to an increase in pH, counteracts the acid addition caused by manganese dioxide deposition during charging. This also explains the lower pH drift observed during the charging process compared to the discharging process in Fig. 5b. It suggests that the protons involved in the reaction at the manganese dioxide positive electrode align with the theoretical values, supporting the assumption that this reaction is the main process at play.

To assess the influence of the zinc electrode on pH, a long-term measurement test is conducted (Fig. 6b). A rapid increase in pH, reaching approximately pH 5, is observed, which could be assigned to a significant corrosion of the zinc anode due to hydrogen

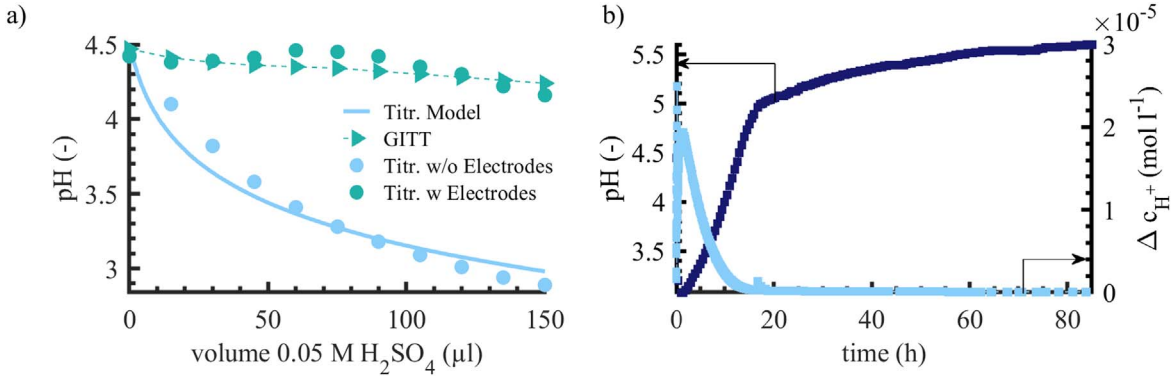

Figure 6. Influence of hydrogen evolution on pH behavior. (a) Comparison of the titration model with sulfuric acid titration experiments, as well as GITT measurements and titrations with electrodes. The results indicate that hydrogen evolution contributes to the higher pH. (b) pH evolution and corresponding proton concentration change, highlighting the impact of hydrogen evolution on the zinc electrode in sulfate electrolyte.

evolution (leading to proton loss).[53] Subsequently, a smaller change in proton concentration is seen, followed by a saturation point around pH 5.3, which can be linked to the buffering effect of the precipitation of ZHS and is consistent with the findings of Zhang et al.[48,49]

In summary, it can be concluded that by incorporating speciation, the equilibrium potential of the reaction is well simulated. It was demonstrated that, contrary to the prevailing opinion, the complexation behavior of acetate and sulfate anions has only a minor influence on the open-circuit voltage, whereas pH has a significantly larger effect. Due to its much lower buffer capacity, much greater pH fluctuations are observed in the sulfate electrolyte under the same operating conditions compared to the acetate electrolyte. It was also shown that the addition or removal of protons through manganese dioxide deposition can be simulated by titration, provided that the proton removal through hydrogen evolution at the anode is also considered.

Mass transport as limiting step.—In the previous analysis, it was demonstrated that the equilibrium behavior remains consistent across different anion species. Building upon these findings, the following study focuses on operational conditions, where the role of the electrolyte becomes more complex and is governed by non-equilibrium kinetic processes. During operation of the ZMB cell, the coupling between reaction and mass transport needs to be investigated to understand the underlying mechanism. To investigate this, an experiment was conducted in which ion transport conditions were systematically varied. Specifically, the ZMB cells were cycled under two conditions: with and without mechanical stirring (Fig. 7, dashed and solid line). In both cases, the pH was adjusted to 4.5 by the addition of sulfuric acid to ensure consistency between the electrolytes. Generally, at the electrode interfaces, mass transfer primarily occurs through diffusion. The introduction of stirring induces convective mass transport, enhancing ion transport to the electrode surface and increasing local concentrations to avoid concentration gradients by limited diffusion between the electrodes/in the electrolyte.

Figures 7a and 7b show the voltage curves based on sulfate and acetate at a current density of 0.06 mA.cm^{-2} and 0.06 mAh cm^{-2}, with and without stirring. For the sulfate-containing electrolyte, a continuous voltage drop is observed during the discharge step, followed by a characteristic voltage dip and a subsequent voltage plateau at approximately 1.3 V. This plateau has been associated with the precipitation of ZHS.[54] When stirring is introduced, the voltage plateau for the sulfate-based electrolyte changes significantly, exhibiting a distinct reduction in overpotential with forced convection while the characteristic voltage dip disappears.

In contrast, for the acetate-based electrolyte, a lower discharge capacity for the stirred solution, is observed, a phenomenon that will be discussed in detail in a later section. Furthermore, it exhibits a well-defined, stable voltage plateau throughout the entire discharge process, which remains unchanged upon stirring. This suggests that mass transport limitations affect the sulfate-based electrolyte but do not play a significant role in the acetate-based system. Given that Zn^{2+} and Mn^{2+} concentrations in this pH range are significantly higher than that of protons, it is reasonable to assume that proton transport becomes the rate-limiting factor, while acetate supports pH stability in acetate-based electrolyte. As a result, pronounced pH gradients form at the electrode surface in the sulfate-based electrolyte, which can be mitigated through electrolyte mixing. These findings also suggest that the primary determinant of electrochemical behavior is not the complexation properties of the anions but rather their pH-buffering capacity.

To test this hypothesis, the pH dependence of these properties (s. section physicochemical properties), is utilized. Figure 8a illustrates

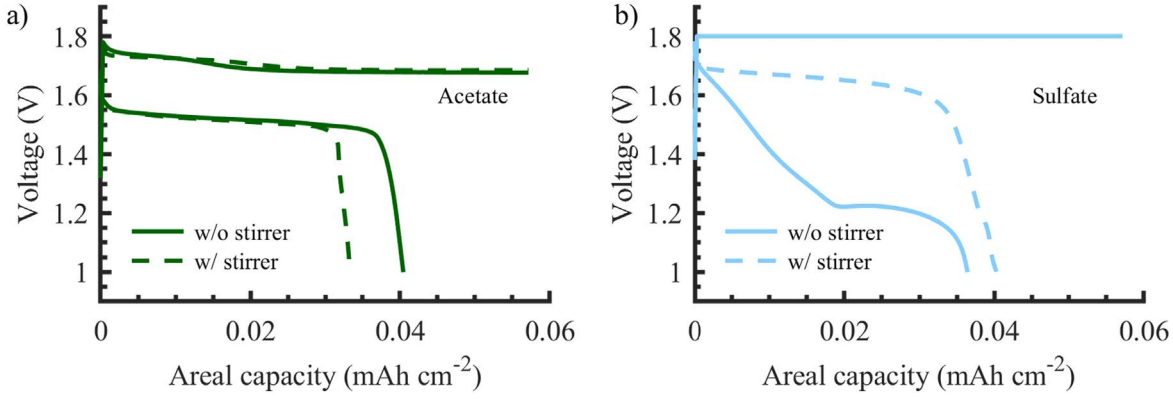

Figure 7. Influence of transport conditions on electrochemical performance. (a) No significant voltage difference for acetate-based electrolyte under stirred and unstirred conditions. (b) Pronounced changes in the voltage plateau for sulfate-based electrolyte, highlighting the transport of species as a limiting factor.

the buffer capacity for 1 M $ZnAc_2$ and 1 M $MnAc_2$, where a clear decrease in buffer capacity is observed as the pH increases from 4.5 to 6. As shown in Fig. 8b, the corresponding voltage curve for the first cycle over the rated capacity is shown, where the pH is adjusted to the target pH of 5.3 and 4.5 with sulfuric acid. The choice of pH 5.3 was made to explore an intermediate state between pH 4.5 and 6, allowing for a comparative analysis of the effects observed within this range. Firstly, a decreasing voltage with increasing pH can be determined, which is consistent with the pH dependence of the Nernst equation. A notable change in the curve characteristics is also observed. The constant voltage profile at pH 4.5 distinctly differs from the profiles at pH 5.3 and pH 6, which exhibit multiple plateaus, reminiscent of the sulfate-based electrolyte's behavior. This voltage drop is likely associated with the precipitation of ZHA, a phenomenon that has been scarcely addressed in recent publications.[47] The results suggest that the decreasing buffer capacity at higher pH values could play a role in the observed changes in the electrochemical behavior. Additionally, the changes in the potential curve with increasing mass transport via forced convection further support this hypothesis (Fig. 8c). Furthermore, chronoamperometry measurements are carried out to compare the limiting currents (Fig. 8d). A fixed potential of 1. 8 V was applied to the working electrode and the current response was measured as a function of time. The results demonstrate a significant dependence of current density on the buffer system and its pH relative to its pK_a. While sulfate at pH 4.5 serves as a reference to compares the influence of the proton concentration without buffer capacity and exhibits a consistently low current, acetate buffers show pronounced differences. Notably, the current density for acetate at pH 4.5 is significantly higher than at pH 6. This indicates that the higher current at pH 4.5 cannot be attributed solely to proton concentration, but rather reflects the higher buffering capacity of the system near its pK_a. At this point, efficient proton uptake by the buffer mitigates the local acidification resulting from Mn^{2+} oxidation. In contrast, at pH 6 and pH 5.3, protons accumulate more rapidly near the electrode surface, leading to a local pH drop that hinders the reaction and manifests as a lower current density. Figure S4 illustrates the polarization behavior of the zinc electrode relative to the zinc reference, confirming that the observed current differences mainly originate from processes at the cathode.

It can be summarized that the pH of 6 compared to pH 4.5 when using acetate-based electrolytes leads to reduced performance with respect to reversibility and overpotential. Nevertheless, it should also be noted that additional factors, such as pH-dependent kinetics and the formation of further manganese oxides at elevated pH cannot be entirely excluded. Despite this, these pH conditions are frequently reported in the literature for proton-dependent processes, even though their limited proton supply diminishes their practical relevance.[47] These findings highlight that the interplay between buffer composition, protonation state, and pH critically influences the electrochemical performance.

Influence of anion and pH on reversibility of MnO_2 deposition.—In the following, the concentration of Ac^- are continuously varied from 0 to 0.2 to 1 M Ac^- in order to check their influence. Even the slight addition of acetate (0.2 M Ac^-) leads to a significant stabilization of the potential curve at constant pH (Fig. 9a). The behavior is very similar to the curve for the addition of 1 M Ac^-, for which only slightly higher overvoltage during charging and an earlier drop in the discharge voltage can be observed. When compared with the acetate-free electrolyte (0 M Ac^-), a significant difference in the shape of the curve is visible and the two-plateau discharge behavior becomes a continuous profile.

Major differences between electrolytes become apparent (Fig. 9b) as soon as the areal capacity and current density are increased (from 0.06 mAh cm^{-2}, 0.06 mAh cm^{-2} to 1 mA cm^{-2}, 1 mAh cm^{-2}). For the acetate-free electrolyte, a clear increase in the voltage for charging and discharging can be seen. It should also be

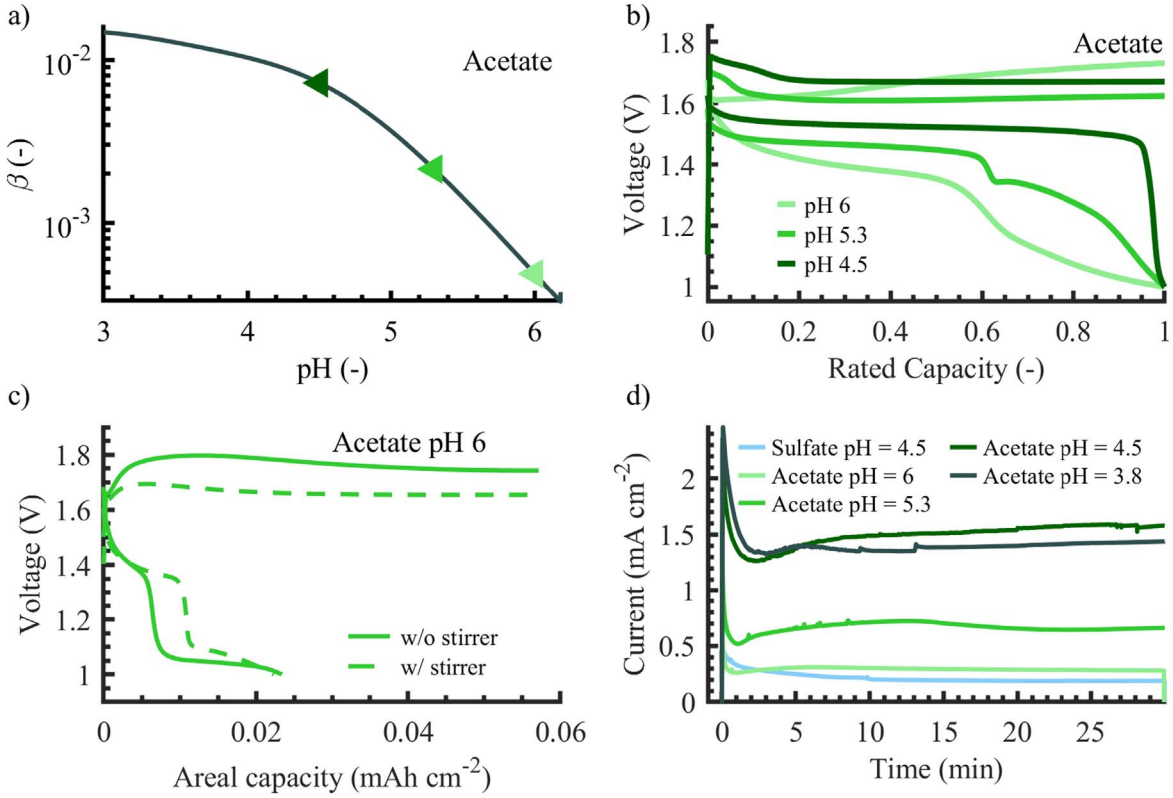

Figure 8. Influence of pH on buffer capacity for acetate based electrolyte (4 M Ac^-). (a) Buffer capacity as a function of pH. (b) Corresponding electrochemical behavior at different pH values. (c) Influence on transport conditions on acetate electrolyte at pH = 6. (d) Chronoamperometry measurements for acetate electrolyte at various pH values.

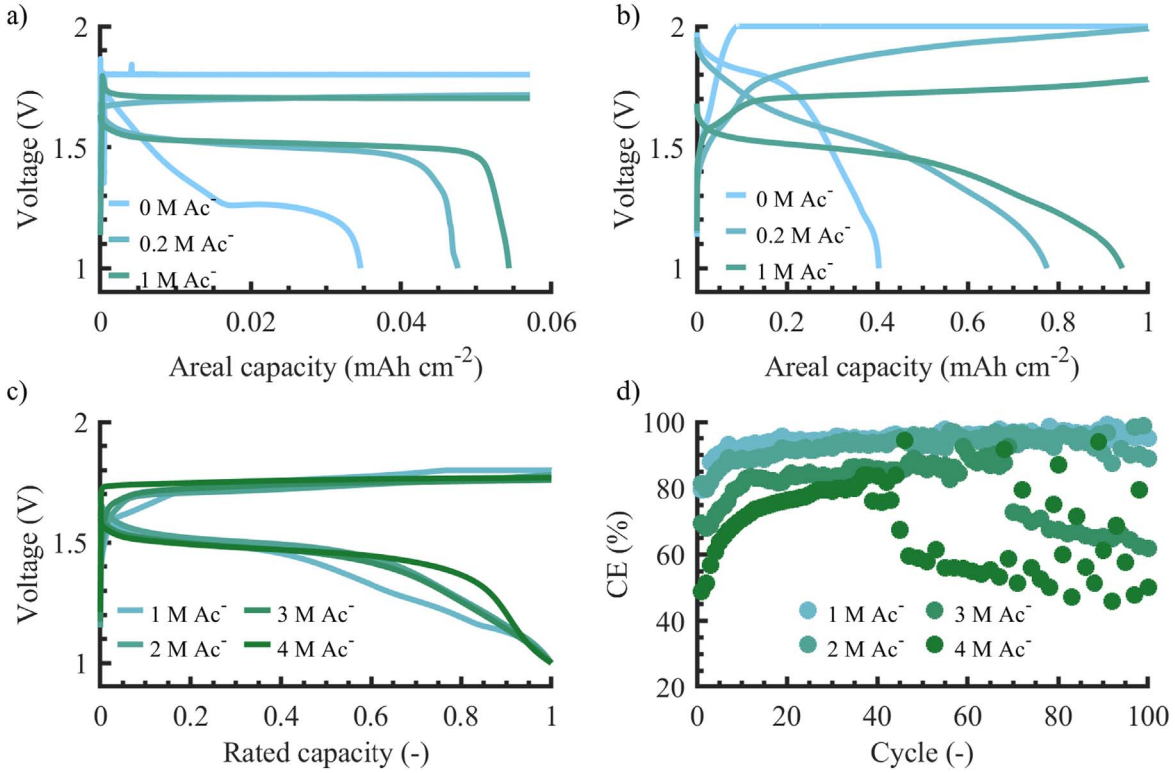

Figure 9. Influence of the acetate content on the galvanostatic charge-discharge profiles for (a) 0, 0.2 and 1 M Ac^- at 0.06 mA cm^{-2} and 0.06 mAh cm^{-2}. (b) 0, 0.2 and 1 M Ac^- at 1 mA cm^{-2} and 1 mAh cm^{-2}. (c) 1, 2, 3 and 1 M Ac^- at 1 mA cm^{-2} and 1 mAh cm^{-2}. (d) Long-term cycling performance at 1 mA cm^{-2} and 1 mAh cm^{-2}.

noted that the charge voltage limit had to be raised from 1.8 V to 2 V in order to enable target capacity of 1 mAh.cm^{-2}. This can be explained by large pH changes on the surface. According to the Nernst equation, a pH about 2 at the surface is sufficient to reach the final charge voltage by the pH effect alone, without taking other kinetic effects into account and is thus inhibited further reaction (Fig. 4c). A similar, albeit not quite as pronounced, behavior is noticeable for the 0.2 M electrolyte, whereas a much smaller change can be seen for the 1 M Ac^- electrolyte. Overall, it can therefore be stated that the pH stabilization depends on the current density and the composition of the electrolyte with different Ac^- concentrations.

Subsequently, the concentration of acetate in the electrolyte is successively further increased until the entire salt is added by acetate salts (4 M). Figure 9c shows the voltage curve for an areal capacity of 1 mAh.cm^{-2} in relation to the total charge/discharge capacity in order to facilitate proper interpretation. Although the exclusively acetate-based electrolyte shows a relatively flat curve that only bends towards the end of the discharge, a flattening behavior towards the end of the discharge voltage curve can be seen as the sulfate content increases. A similar behavior can be observed for charging voltage behavior at the beginning of the charging phase. Moreover, a decrease in coulombic efficiency can be observed with increased acetate concentration (Fig. 9d). To explain this observation, the reaction pathways for the MnO_2 deposition are studied in the following.

The different behavior of the Coulombic efficiency for increased Ac^- concentrations in the electrolyte could be attributed to two different prevailing reaction pathways for MnO_2 deposition reaction that are described in literature (Fig. 10). During the MnO_2 deposition, the oxidation state of the manganese ion changes from Mn^{2+} over Mn^{3+} to Mn^{4+}, when Mn(IV)O_2 is formed. A special role is played by the stability of the Mn^{3+} intermediate, which is formed in the first step of the charging process.[55] If Mn^{3+} is unstable, it easily hydrolyzes to form MnOOH, which precipitates on the positive electrode. This MnOOH undergoes further solid-state oxidation to generate MnO_2. In contrast, if Mn^{3+} is sufficiently stable, it can diffuse away from the electrode and undergo disproportionation. The Mn^{4+} subsequently hydrolyzes to MnO_2, which precipitates onto the electrode surface or remaining suspended in the electrolyte solution.[22,56] Although these pathways are described as distinct mechanisms, the oxidation reaction typically proceeds through a combination of both. The relative preference for each pathway is dictated by the stability of Mn^{3+}, which is determined by the specific properties of the electrolyte.[57] Some publications show that Ac^- can stabilize the Mn^{3+} intermediate, which can diffuse away and is no longer available as active material. This is in line with the observation that with increasing acetate concentration more electrolytic products are dispersed into the electrolyte solution, leading to a brownish turbidity of the electrolyte (Fig. S5). The fact that an increase in mass transport through (forced) convection leads to reduced capacity can also be seen as confirmation of this thesis (Fig. 7a), however, additional effects may also contribute to the observed behavior. It should also be added that the chemical dissolution of MnOOH while MnO_2 reduction can also be responsible for inactive manganese species.[58]

Moreover, an increase in coulombic efficiency is observed during the first few cycles (Fig. 9d, a phenomenon that has also been reported in previous studies and is attributed to the formation of inactive MnO_2, often referred to as "dead MnO_2".[14,59] This not only alters the electrode's surface characteristics but also modifies its nucleation properties, thereby influencing the deposition process and overall electrode performance. For instance, Mateos et al. documented an almost twofold increase in mass within the first 10 cycles.[32] This accumulation of MnO_2 is accompanied by a decrease in pH, which can be attributed to the release of protons during the deposition process.[54] One explanation for the remaining material could be that during the reduction of MnO_2, the electrochemical or chemical dissolution of the MnOOH formed on the interface breaks the electronic connection.[58] The observed activation process appears to be linked to changes in the electrode surface. Experimental

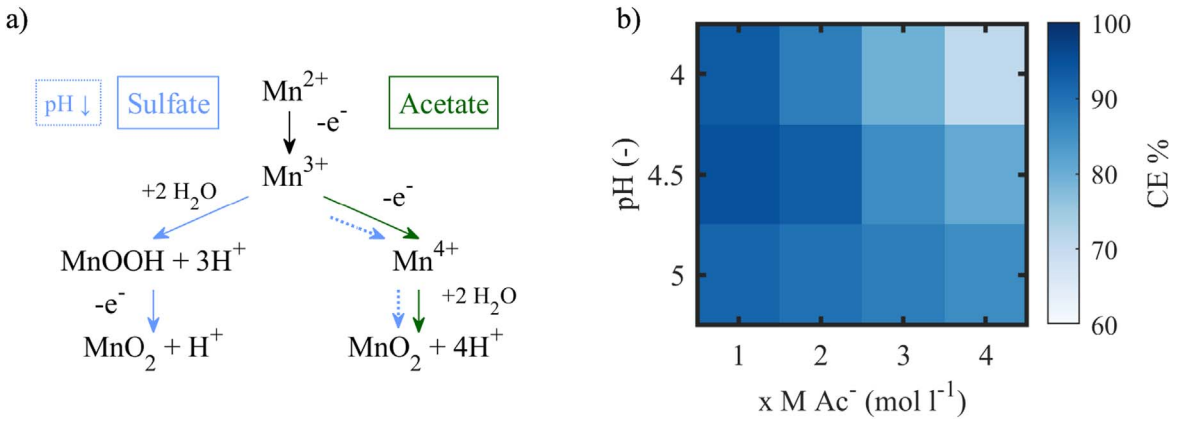

Figure 10. (a) Schematic representation of the favored reaction pathways of MnO_2 deposition for different anions. (b) Effect of acetate concentration and pH on the CE. As the acetate content increases, the process increasingly follows the right pathway, leading to a decrease in CE. Additionally, lower pH further promotes the right pathway.

evidence suggests that, for electrodes coated with manganese dioxide, the lattice match between MnO_2 and MnOOH promotes the precipitation pathway.[57] In acetate-based electrolytes, where the disproportionation reaction is predominant, surface modifications have a more pronounced effect on the reaction dynamics. In contrast, in sulfate-based electrolytes, where the precipitation pathway is already more dominant, such changes exert a comparatively smaller influence. This underscores the fact, that in addition to the electrolyte conditions, the electrode surface also plays a decisive role in the stabilization of the Mn^{3+} intermediate.

Another important influencing factor is the pH of the solution. Wang and colleagues show that a low pH value (3.2) further increases the disproportionation mechanism for acetate-based electrolytes.[60] Other publications also show that brown discoloration due to disproportionation can also be observed in sulfate-based electrolytes at even more acidic pH values.[58,61,62] Here, the stabilization of Mn^{3+} is achieved by the hydrolysis reaction with $pK_a = 0.03$, in connection to the following chemical reaction:[63]

$$[Mn(H_2O)_6]^{3+} \rightleftharpoons [Mn(H_2O)_5(OH)]^{2+} + H^+ \quad [8]$$

In the following, the effects of varying the initial pH within the target range of 4 to 5 are examined. Each cell undergoes 100 cycles at 1 mAh.cm^{-2} and 1 mA.cm^{-2}. Regardless of pH, a higher acetate content consistently leads to a decrease in coulombic efficiency (Fig. 10b). Since the cells in this study utilize zinc foil with a high capacity excess, these changes in efficiency primarily reflect variations in the cathode reaction, while effects on the anode are discussed in the following section. Moreover, the influence of the initial pH becomes more pronounced with increasing acetate content. For high acetate concentrations, lower pH values correlate with reduced reversibility, which aligns with Wang et al.'s findings.[60] However, while Wang et al. investigated the impact of pH at a constant acetate concentration, the results of this study suggest that increasing acetate content amplifies this effect. This could indicate that even a slight decrease in pH enhances the stabilization of Mn^{3+}, thereby promoting the formation of inactive MnO_2.

At lower acetate concentrations, coulombic efficiency reaches an optimum at pH 4.5. This may be since at pH 5, the precipitation of hydroxides during electrochemical cycling becomes increasingly likely. Additionally, studies have shown that higher pH levels favor the formation of zinc-containing manganese oxides,[49,60] which are suspected to reduce reversibility and significantly lower electrical conductivity.

The findings emphasize the crucial interplay between electrolyte composition and key operational parameters such as pH, current density, charge voltage and specific capacity in optimizing energy density and cycle performance. Although nearly 100% coulombic efficiency was observed under semi-equilibrium conditions with minimal differences between anions, substantial variations emerged under dynamic conditions. These findings suggest that optimal acetate-to-sulfate ratios must balance the pH stability benefits of acetate with the higher efficiency and reliability offered by sulfate. Furthermore, these results highlight the necessity of maintaining consistent experimental conditions, as variations in key parameters can lead to divergent interpretations. Further advancements in controlling Mn^{3+} complex behavior could lead to improved electrolyte formulations that harness the benefits of both anion types. Studies suggest that redox mediators may help recover lost active species,[58] though mitigating self-discharge caused by the "shuttle effect" remains a challenge that requires further investigation.[64] Another promising approach involves diffusion barriers to limit the dispersion of reactive species within the electrolyte.[56] Additionally, this study reaffirms that cell chemistry is highly sensitive to even small pH variations. Spatially resolved models could provide deeper insights into these complex interactions and their impact on battery performance. Future research should explore the effects of varying operational conditions, such as current density and temperature fluctuations, to assess the robustness of observed mechanisms. Investigating alternative buffering agents could further enhance electrochemical stability, ultimately leading to optimized electrolyte formulations that improve both efficiency and longevity in ZMBs.

Influence of the anions and the pH on the zinc anode.—To verify the effects of anion and pH on zinc anode cycling stability, we compared the Zn plating/ stripping performance of asymmetric Cu|| Zn cells at a current density of 1 mA.cm^{-2} and an areal capacity of 1 mAh.cm^{-2}. To eliminate the pH-related influences, all electrolytes were adjusted to a pH 4.5. The charging and discharging behavior for the 50th cycle is shown as an example (Fig. 11a). A rising voltage hysteresis and a decline in reversibility were observed with increasing acetate content. This trend can be attributed to the decreasing conductivity of the electrolyte with higher acetate concentrations. An estimate of this effect is provided in Supporting Information S1. Additionally, a higher acetate content correlates with a reduction in discharge capacity.

This observation is further supported by the average coulombic efficiency over 100 cycles, which exhibits a linear decrease from sulfate-containing to acetate-containing electrolytes (Fig. 11b). Measurements were repeated three times for each acetate concentration. The trend is also reflected in the increased hydrogen evolution in cycled pouch cells, as observed in symmetric Zn||Zn cells at a current density of 1 mA.cm^{-2} and an areal capacity of 1 mAh.cm^{-2} (Supporting Information Fig. S6). A possible explanation is that buffer addition reduces the electrochemical stability window in the neutral pH range.[65,66]

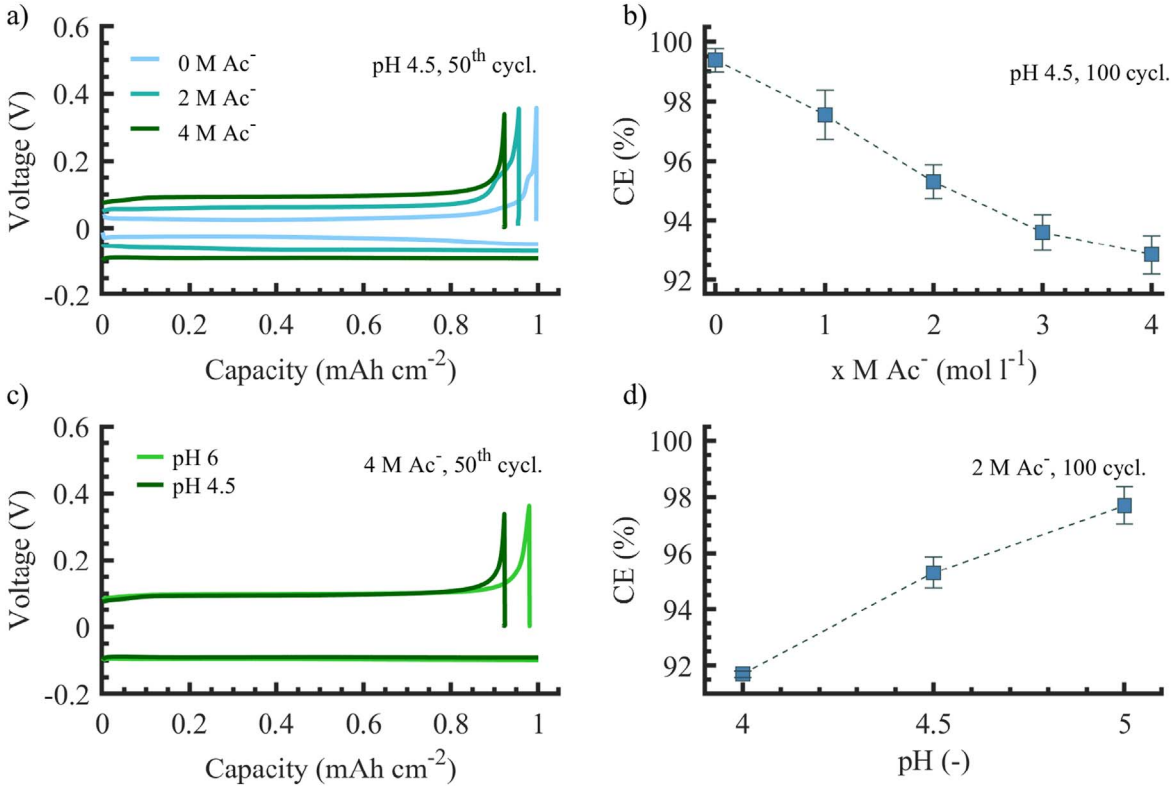

Figure 11. Zn anode reversibility in Zn||Cu cells at 1.0 mA cm^{-2} and 1.0 mAh cm^{-2} as a function of pH and acetate concentration. (a) Stripping/plating profiles at pH 4.5 with varying acetate concentrations (0, 2, 4 M Ac^-) at the 50th cycle. (b) Mean CE over 100 cycles for different acetate concentrations at pH 4.5. (c) Stripping/plating profiles for pH 4.5 and 5 at 4 M Ac^- (50th cycle). (d) Mean CE over 100 cycles for different pH values at 2 M Ac^-.

However, this contradicts several studies reporting reduced hydrogen evolution and improved reversibility for acetate-based electrolytes.[13,33–35,67] Proving our study, Sun et al. similarly investigated the zinc anode stability at different acetate concentrations and found that the highest reversibility was achieved with the lowest acetate content, whereas increasing acetate levels impair the performance.[33] We propose that these inconsistencies observed in the literature arise from variations in the initial pH control of the respective electrolyte composition. To address this, we also examined the effect of the initial electrolyte pH. Raising the pH of the acetate-based electrolyte to 6, according to the publication by Zeng and Xie,[13,20] resulted in a significantly higher discharge capacity while maintaining overvoltage stability (Fig. 11c).

This supports the hypothesis that discrepancies in anode arise primarily from differences in pH control. Still, as discussed in the previous sections, the pH range of pH 6 is associated with the formation of irreversible solids by precipitation reactions and could prove problematic for long-term stability. The influence of the pH range between 4 and 5, which is discussed as optimal with regard to pH, was therefore also investigated. A linear increase in plating and stripping performance can be seen in Fig. 11d in the range between pH 4 and 5 for 2 M Ac^-. This finding underscores the challenge of balancing anodic stability with cathodic conversion efficiency.

Conclusions

This study provides new insights into the interplay of pH, anion composition, and complex behavior in electrolytic ZMB, focusing on acetate- and sulfate-based electrolytes. By developing and validating a thermodynamic model, it is demonstrated that the formation of complexes with the cations significantly shifts the effective range of pH stabilization. Contrary to the opinion of some publications, it has been shown that it is not the complex effect but the increased buffering property of the acetate ions that leads to an altered electrochemical property. Experimental results confirmed that the transport of protons is the rate-limiting step in sulfate-based electrolytes, while acetate anions improve pH stabilization near the electrode interface, facilitating proton-coupled electron transfer mechanisms. Furthermore, these findings underscore the importance of precise pH adjustment in acetate-based electrolytes. Although pH 6 is commonly used for acetate electrolytes in literature, this range provides only limited buffering capacity and electrochemical performance, making it crucial to optimize pH conditions for improved electrochemical stability. For the first time, the acetate content was simultaneously analyzed as a function of pH. Experiments show that increasing the acetate content in the electrolyte correlates with a reduction in coulombic efficiency due to the stabilization of Mn^{3+} intermediates, leading to an accumulation of inactive MnO_2 species. Specifically, acetate-buffered electrolytes support more efficient manganese dioxide deposition while mitigating anode stability issues commonly observed in strongly acidic environments. However, higher acetate concentrations negatively impact reversibility due to enhanced Mn^{3+} complex stabilization, emphasizing the need for a balanced electrolyte design. Contrary to the prevailing opinion, the zinc stability in acetate electrolytes is strongly pH-dependent and less anode-friendly compared to sulfate electrolytes for the same pH conditions.

Acknowledgments

The project on which is publication is based was funded by the German Federal Ministry for Economic Affairs and Energy under grant no. 03EI3040D and German Federal of Education and Research under grant no. 03SF0702B. The Author is responsible for the content of this publication.

ORCID

J. Pross-Brakhage https://orcid.org/0009-0000-1614-8542
J. Meyer https://orcid.org/0009-0001-9798-3052
C. Mehlich https://orcid.org/0009-0003-6984-7349

O. Fitz https://orcid.org/0000-0002-5659-0295
P. Birke https://orcid.org/0000-0002-9679-2369

References

1. J. Pross-Brakhage, O. Fitz, C. Bischoff, D. Biro, and K. P. Birke, *Batteries*, **9**, 367 (2023).
2. Y. Ren, H. Li, Y. Rao, H. Zhou, and S. Guo, *Energy Environ. Sci.*, **17**, 425 (2024).
3. Y. Liao, C. Yang, J. Bai, Q. He, H. Wang, H. Chen, Q. Zhang, and L. Chen, *Chem. Sci.*, **15**, 7441 (2024).
4. L. Li, T. K. A. Hoang, J. Zhi, M. Han, S. Li, and P. Chen, *ACS Appl. Mater. Interfaces*, **12**, 12834 (2020).
5. L. Godeffroy, I. Aguilar, J. Médard, D. Larcher, J.-M. Tarascon, and F. Kanoufi, *Adv. Energy Mater.*, **12**, 2200722 (2022).
6. X. Chen, W. Li, D. Reed, X. Li, and X. Liu, *Electrochem. Energy Rev.*, **6**, 33 (2023).
7. Y. Li, Y. Li, Q. Liu, Y. Liu, T. Wang, M. Cui, Y. Ding, H. Li, and G. Yu, *Angew. Chem. Int. Ed.*, **63**, e202318444 (2024).
8. A. Valinejad, M. Ghafari, Z. Sanaee, and M. Kolahdouz, *J. Mater. Chem. A*, **12**, 31959 (2024).
9. O. Fitz, C. Bischoff, M. Bauer, H. Gentischer, K. P. Birke, H.-M. Henning, and D. Biro, *ChemElectroChem*, **8**, 3553 (2021).
10. O. Fitz, F. Wagner, J. Pross-Brakhage, M. Bauer, H. Gentischer, K. P. Birke, and D. Biro, *Energy Technology*, **11**, 2300723 (2023).
11. H. Yang, D. Chen, R. Zhao, G. Li, H. Xu, L. Li, X. Liu, G. Li, D. Chao, and W. Han, *Energy Environ. Sci.*, **16**, 2910 (2023).
12. Z. Liu, L. Li, L. Qin, S. Guo, G. Fang, Z. Luo, and S. Liang, *Advanced materials (Deerfield Beach, Fla.)*, **34**, e2204681 (2022).
13. X. Zeng, J. Liu, J. Mao, J. Hao, Z. Wang, S. Zhou, C. D. Ling, and Z. Guo, *Adv. Energy Mater.*, **10**, 1904163 (2020).
14. L. Meng, X. Ji, M. Li, T. Liu, W. Dong, Y. Pan, L. Huang, and S. Cheng, *Surfaces and Interfaces*, **29**, 101782 (2022).
15. D. Nakhaie and E. Asselin, *J. Electrochem. Soc.*, **164**, C758 (2017).
16. N. Zhang, F. Cheng, Y. Liu, Q. Zhao, K. Lei, C. Chen, X. Liu, and J. Chen, *J. Am. Chem. Soc.*, **138**, 12894 (2016).
17. F. Wang, O. Borodin, T. Gao, X. Fan, W. Sun, F. Han, A. Faraone, J. A. Dura, K. Xu, and C. Wang, *Nat. Mater.*, **17**, 543 (2018).
18. C. You, R. Wu, X. Yuan, L. Liu, J. Ye, L. Fu, P. Han, and Y. Wu, *Energy Environ. Sci.*, **16**, 5096 (2023).
19. Z.-F. He, Y.-T. Lu, T.-C. Wei, and C.-C. Hu, *ChemSusChem*, **16**, e202300259 (2023).
20. C. Xie, T. Li, C. Deng, Y. Song, H. Zhang, and X. Li, *Energy Environ. Sci.*, **13**, 135 (2020).
21. Z. Zhong, J. Li, L. Li, X. Xi, Z. Luo, G. Fang, S. Liang, and X. Wang, *Energy Storage Mater.*, **46**, 165 (2022).
22. Z. Liu, Y. Yang, B. Lu, S. Liang, H. J. Fan, and J. Zhou, *Energy Storage Mater.*, **52**, 104 (2022).
23. S. Liu, W. Chen, F. Kong, W. Tong, Y. Chen, and S. Chen, *J. Electrochem. Soc.*, **170**, 30545 (2023).
24. C. F. Bischoff, O. S. Fitz, J. Burns, M. Bauer, H. Gentischer, K. P. Birke, H.-M. Henning, and D. Biro, *J. Electrochem. Soc.*, **167**, 20545 (2020).
25. Z. Liu, Y. Yang, S. Liang, B. Lu, and J. Zhou, *Small Struct.*, **2**, 2100119 (2021).
26. D. Chao, W. Zhou, C. Ye, Q. Zhang, Y. Chen, L. Gu, K. Davey, and S.-Z. Qiao, *Angew. Chem. Int. Ed.*, **58**, 7823 (2019).
27. G. Li et al., *Adv. Energy Mater.*, **10**, 1902085 (2020).
28. D. Wu et al., *J. Mater. Chem. A*, **11**, 16279 (2023).
29. Y.-S. Kim, K. D. Harris, B. Limoges, and V. Balland, *Chem. Sci.*, **10**, 8752 (2019).
30. M. Mateos, K. D. Harris, B. Limoges, and V. Balland, *ACS Appl. Energy Mater.*, **3**, 7610 (2020).
31. V. Balland, M. Mateos, A. Singh, K. D. Harris, C. Laberty-Robert, and B. Limoges, *Small*, **17**, e2101515 (2021).
32. M. Mateos, N. Makivic, Y.-S. Kim, B. Limoges, and V. Balland, *Adv. Energy Mater.*, **10**, 2000332 (2020).
33. J. Sun, Z. Liu, K. Li, Y. Yuan, X. Zheng, Y. Xu, M. Wang, M. Chuai, H. Hu, and W. Chen, *ACS Appl. Mater. Interfaces*, **14**, 51900 (2022).
34. Y. Le Li, M. Xie, R. Yao, X. Cao, Y. Mai, L. Ji, X. Chen, Dong, and Y. Xia, *Chemical communications (Cambridge, England)*, **60**, 6809 (2024).
35. D. Han et al., *Adv. Energy Mater.*, **12**, 2102982 (2022).
36. F. Wan, L. Zhang, X. Dai, X. Wang, Z. Niu, and J. Chen, *Nat. Commun.*, **9**, 1656 (2018).
37. R. N. Goldberg, R. T. Giessmann, P. J. Halling, C. Kettner, and H. V. Westerhoff, *Beilstein J. Org. Chem.*, **19**, 303 (2023).
38. S. Berto et al., *Anal. Chim. Acta*, **1303**, 342476 (2024).
39. S. P. Santoso, I. K. Chandra, F. E. Soetaredjo, A. E. Angkawijaya, and Y.-H. Ju, *J. Chem. Eng. Data*, **59**, 1661 (2014).
40. S. D. Schwoebel, D. Höhlich, T. Mehner, and T. Lampke, *Computation*, **9**, 55 (2021).
41. E. M. Kimani, A. J. B. Kemperman, W. G. J. van der Meer, and P. M. Biesheuvel, *J. Chem. Phys.*, **154**, 124501 (2021).
42. D. S. Smith, *Solution of Simultaneous Chemical Equilibria in Heterogeneous Systems: Implementation in Matlab*, Chemistry Faculty Publications. https://scholars.wlu.ca/chem_faculty/14 (2019) 14.
43. J. Carrayrou, R. Mosé, and P. Behra, *AlChE J.*, **48**, 894 (2002).
44. et al., *ChemSusChem*, **12**, 379 (2019).
45. W. Wang and D. B. Breisinger, *Metall. Mater. Trans. B (Metallurgical and Materials Transactions B)*, **29**, 1157 (1998).
46. A. Krężel and W. Maret, *Arch. Biochem. Biophys.*, **611**, 3 (2016).
47. S. J. Kim, D. Wu, L. M. Housel, L. Wu, K. J. Takeuchi, A. C. Marschilok, E. S. Takeuchi, and Y. Zhu, *Chem. Mater.*, **33**, 7283 (2021).
48. C.-C. Kao, C. Ye, J. Hao, J. Shan, H. Li, and S.-Z. Qiao, *ACS Nano*, **17**, 3948 (2023).
49. O. Rubel, T. N. T. Tran, S. Gourley, S. Anand, A. van Bommel, B. D. Adams, D. G. Ivey, and D. Higgins, *J. Phys. Chem. C*, **126**, 10957 (2022).
50. K. W. Knehr, S. Biswas, and D. A. Steingart, *J. Electrochem. Soc.*, **164**, A3101 (2017).
51. R. Ronen, I. Atlas, and M. E. Suss, *J. Electrochem. Soc.*, **165**, A3820 (2018).
52. M. Li, J. Wang, B. Gou, D. Fu, H. Wang, and P. Zhao, *ACS Omega*, **7**, 9602 (2022).
53. A. Singh, L. Ouassi, K. Allemang, J.-F. Lemineur, O. Sel, F. Kanoufi, and C. Laberty-Robert, *J. Power Sources*, **625**, 235585 (2025).
54. I. Aguilar et al., *Energy Storage Mater.*, **53**, 238 (2022).
55. A. J. Gibson, B. Johannessen, Y. Beyad, J. Allen, and S. W. Donne, *J. Electrochem. Soc.*, **163**, H305 (2016).
56. X. Li, K. Qi, Z. Qin, X. Ding, Y. Zhu, Z. Hou, and Y. Qian, *ACS Nano*, **18**, 27016 (2024).
57. M. F. Dupont, A. J. Gibson, A. Elbourne, M. Forghani, A. D. Cross, and S. W. Donne, *J. Electrochem. Soc.*, **167**, 40520 (2020).
58. X. Ye, D. Han, G. Jiang, C. Cui, Y. Guo, Y. Wang, Z. Zhang, Z. Weng, and Q.-H. Yang, *Energy Environ. Sci.*, **16**, 1016 (2023).
59. J. Lei, Y. Yao, Z. Wang, and Y.-C. Lu, *Energy Environ. Sci.*, **14**, 4418 (2021).
60. H. Wang, T. Wang, G. Stevenson, M. Chamoun, and R. W. Lindström, *Energy Storage Mater.*, **63**, 103008 (2023).
61. H. Guo, L. Wan, J. Tang, S. Wu, Z. Su, N. Sharma, Y. Fang, Z. Liu, and C. Zhao, *Nano Energy*, **102**, 107642 (2022).
62. S. Wu, H. Guo, Z. Su, C. Jia, X. Zhang, S. Wang, T. Zhao, Q. Meyer, and C. Zhao, *Adv. Funct. Mater.*, **34**, 2315706 (2024).
63. F. A. Cotton, G. Wilkinson, C. A. Murillo, and M. Bochmann, *Advanced Inorganic Chemistry* (Wiley, New York, Weinheim) (1999) 9780471199571.
64. M. Li, J. Wu, H. Li, and Y. Wang, *Materials (Basel, Switzerland)*, **17** (2024).
65. T. J. Yokokura, J. R. Rodriguez, and V. G. Pol, *ACS Omega*, **5**, 19715 (2020).
66. A. Dushina, J. Stojadinović, and F. La Mantia, *Enhanced Electrochemical Capacitors Selection of Papers from the 1st International Symposium (ISEE'Cap09)*, **167**, 262 (2015).
67. C. Lin, X. Yang, P. Xiong, H. Lin, L. He, Q. Yao, M. Wei, Q. Qian, Q. Chen, and L. Zeng, *Advanced science (Weinheim, Baden-Wurttemberg, Germany)*, **9**, 2201433 (2022).